JOURNAL OF MATERIALS SCIENCE 31 (1996) 5179–5184

Deformation capability and protective role of zirconia coatings on stainless steel

J. F. QUINSON, C. CHINO,
Laboratoire G.E.M.P.P.M., CNRS UMR 5510, INSA, 20 Avenue Albert Einstein, 69621 Villeurbanne Cédex, France

A. M. DE BECDELIEVRE
Département de Chimie Appliquée, UCB-Lyon I, 43 Bd du 11 Novembre 1918, 69622 Villeurbanne Cédex, France

C. GUIZARD
Laboratoire des Matériaux et Procédés Membranaires, CNRS UMR 9987, ENSC, 8 rue de l'Ecole Normale, 34053 Montpellier Cédex 1, France

M. BRUNEL
Laboratoire de Cristallographie, CNRS, B.P. 166X, 38042 Grenoble Cédex, France

ZrO_2 coatings were obtained by the alkoxide route and deposited on to stainless steel using the dip-coating technique. The starting solutions were prepared by mixing zirconium tetrabutoxide, isopropanol, acetylacetone. The water content for the hydrolytic reaction came from atmospheric moisture. These coatings were characterized by scanning electron microscopy, X-ray fluorescence, Fourier transform–infrared spectroscopy, and X-ray diffraction. Their deformation capability was studied by using the stretch deformation test. It is worth noting that these coatings deposited on stainless steel have the capacity to deform extensively without apparent cracks or fracture. Their ability to protect the metallic substrate against corrosion, in a neutral chloride medium, was investigated. For this purpose, the pitting potential of the coated metal was measured by the potentiodynamic polarization technique and the a.c. impedance diagram of the coating was recorded in the potentiostatic mode at the rest potential. The variation in the pitting potentials revealed a temporary increase in the corrosion resistance of coated stainless steel, which disappeared after ageing of the coatings in the chloride solution. During ageing, the coating resistance deduced from the complex diagram via an equivalent circuit, decreases, thus showing a deterioration.

1. Introduction

For many reasons, especially its low-temperature route, the sol–gel process is an efficient method for preparing ceramic coatings on glasses [1–6], or on metals [7–18].

The reports concerning coatings on metal surfaces that have been published, include mainly studies on the protection of substrates against air oxidation or chemical corrosion.

The aim of this work was to study both the protective action and the deformation capability of zirconia coatings prepared on stainless steel substrates. A knowledge of such properties is very important, taking into account potential industrial applications of these materials. The structural organization of the interphase of this composite system has already been investigated thoroughly by the XPS technique [19].

2. Experimental procedure

Zirconia coatings were prepared by mixing zirconium tetrabutoxide with isopropanol in a 1:5 weight ratio. Then, acetylacetone was added in a 1:1 molar ratio with the zirconium tetrabutoxide. The water content for the hydrolytic reaction originates from the atmospheric moisture above the coating bath.

The substrate used was 304 stainless steel. The stainless steel plates were successively polished with abrasive paper and diamond paste up to 1 μm in order to obtain a polymirror-like surface state, and degreased ultrasonically in acetone.

These stainless steel plates were dipped into the solution and withdrawn at a rate of $10\,cm\,min^{-1}$. Then, the coated plates were thermally treated at 500 °C for 5 min under an air atmosphere. This procedure was repeated several times to prepare thicker coatings, called multi-layered coatings.

The multi-layered coating thickness was determined using the X-ray fluorescence technique. Evaluation was made via intensity measurements of the ZrK_α radiation, which is considered to be directly proportional to the thickness of the ZrO_2 coating under study. The calibration factor relating thickness to the measured intensity was derived from monolayered coatings whose thicknesses were determined

0022–2461

by ellipsometry. The morphology and microstructure of coatings were, respectively, determined by scanning electron microscopy (SEM), Fourier transform-infrared (FT–IR) spectroscopy, and X-ray diffraction (XRD).

Their deformation capability and adherence to the substrate were, respectively, evaluated by the stretch deformation test and the scotch tape test, the latter being a qualitative method. Information about the way in which the coatings accommodate the imposed strain was obtained by SEM analysis.

Finally, their protective role with regard to the stainless steel substrate was estimated through the corrosion behaviour of the metal, in neutral chloride solution. Both the rest potential, E_a, and the pitting potential, E_p, of the electrode (coated substrate) were measured in de-aerated 0.5 M NaCl solution. The current–voltage curves obtained in the potentiokinetic mode (15 mV min^{-1}), after maintaining the electrode at -500 mV/SCE as the initial potential for 5 min, allow the determination of E_p from the usual rapid current growth associated with pit development on stainless steel. The larger the value of E_p, the higher is the pitting corrosion resistance of stainless steel.

Furthermore, a.c. impedance measurements were carried out in order to study ageing of zirconia coatings in the chloride environment. The a.c. impedance diagrams were recorded with a Tacussel Z Computer, at the rest potential and over the frequency range 10^5–10^{-3} Hz. The electrolyte used was a neutral, aerated or de-aerated, 0.5 M or 0.02 M NaCl solution.

3. Results and discussion

3.1. Morphology and microstructure

Up to four layers of zirconia, e.g. at a thickness of 0.15 μm, crack-free and homogeneous coatings were prepared as shown in Fig. 1.

In the firing conditions, organic-free and crystalline ZrO_2 coatings were obtained. Fig. 2 illustrates the evolution of FT–IR spectra of coatings with the heat treatment. Before firing, the absorption bands due to Zr–O–C and C–H bonds were, respectively, observed near (◆) 1560–1450 cm^{-1} and (◇) 2950 cm^{-1}; the strong absorption band at (●) 1620 cm^{-1} was assigned to the acetylacetone ligand in the enol form; finally the IR spectrum shows an absorption band at (△) 720 cm^{-1}, characteristic of Zr–O–Zr bonds. After firing, all the absorption bands attributed to organic groups had disappeared, while the band assigned to Zr–O–Zr bonds remained and became more intense.

Fig. 3 shows the temperature evolution of the XRD patterns of coatings. At 400 °C, the broad, weak peak observed at 15.70°, was typical of amorphous zirconia. From 500 °C onwards, the peaks present at 15.19° and 17.69° were due to crystalline zirconia. Because only one peak was detectable over the range 17°–18°, it was assumed, taking the data of Table I into consideration, that zirconia was in the cubic phase. This crystalline state, which theoretically characterizes zirconia at high temperature, has already been noted at low temperature [20]. After firing at 600 °C, the cubic zirconia peaks were still present along with an additional peak

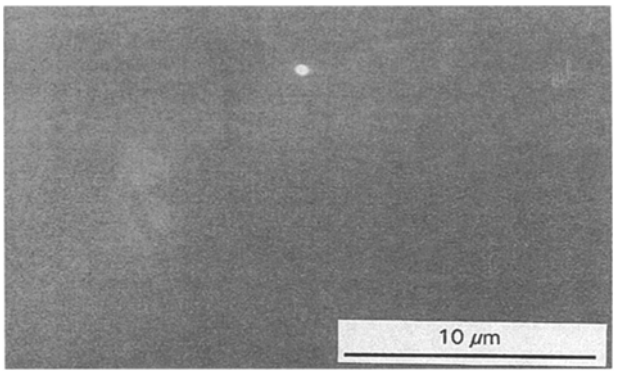

Figure 1 Scanning electron micrograph of a zirconia four-layer coating.

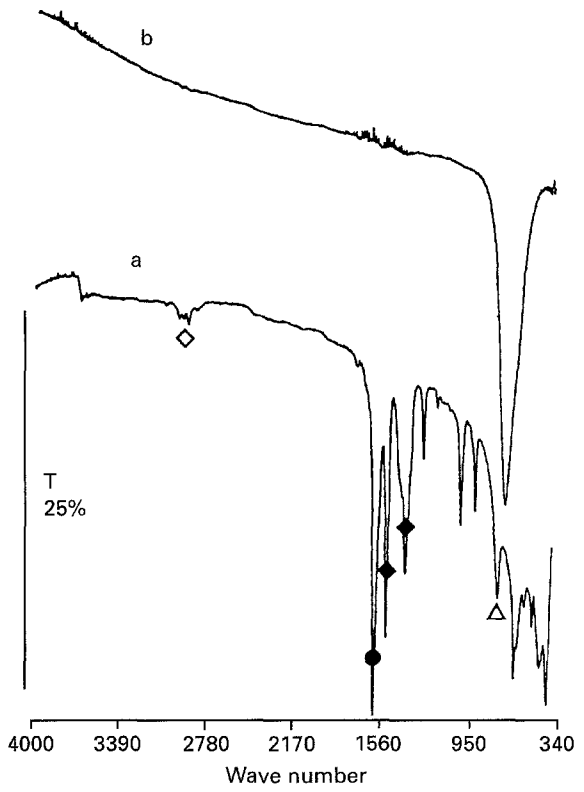

Figure 2 FT–IR spectra of zirconia coatings (a) before and (b) after heating.

at 16.53° attributed to the iron oxide, Fe_2O_3 (ASTM 33-664). This last result reveals that iron in the oxidized state diffuses into the ceramic during heat treatment. Whatever the heat treatment, two peaks were always observed at 21.9° and 22.4°. They were, respectively, assigned to the austenitic phase of the substrate and to a martensitic layer produced at the surface by polishing [21].

From X-ray diffraction patterns, Scherrer analysis indicated that the zirconia coatings were comprised of fine particles. The mean crystal size varied only between 8.5 and 9.5 nm from 500–600 °C.

3.2. Deformation capability

Scanning electron micrographs of zirconia monolayer and four-layer coatings on stainless steel, deformed by 5% and 20% elongation, are shown in Figs 4 and 5. The larger the imposed deformation, the more

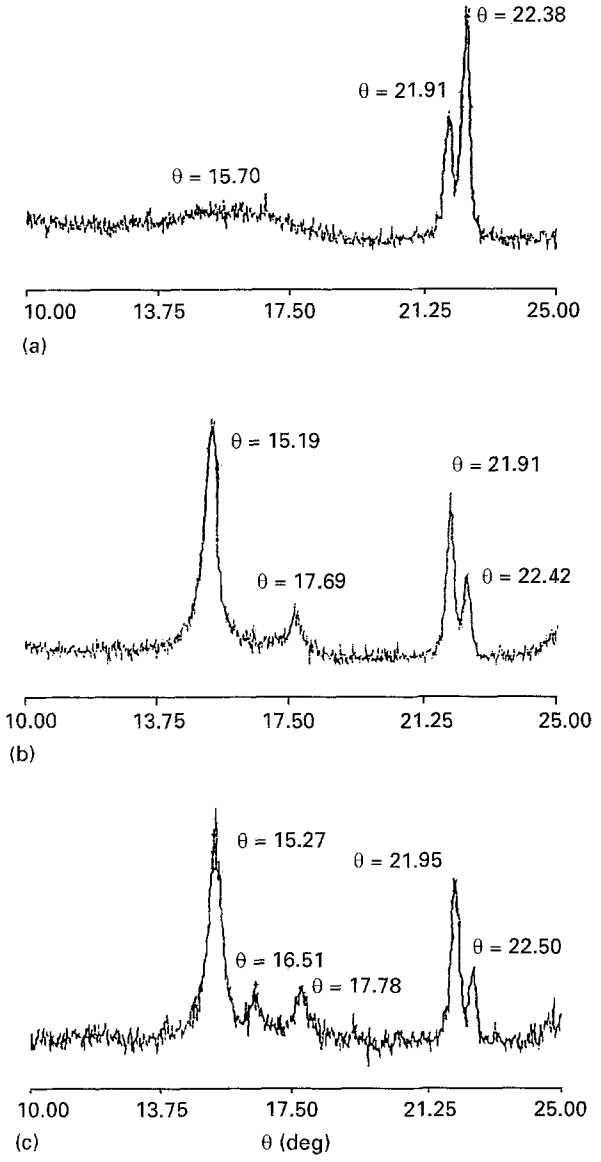

Figure 3 X-ray patterns from zirconia coatings treated at (a) 400 °C, (b) 500 °C, and (c) 600 °C.

TABLE I X-ray diffraction data corresponding to cubic and tetragonal zirconia

	I/I_0	hkl	θ (deg)	I/I_0	hkl	θ (deg)
Cubic zirconia (ASTM 27-997)	100	111	15.25	25	200	17.60
Tetragonal zirconia (ASTM 17-923)	100	111	15.08	18	002	17.23
				25	200	17.65

visible was the emergence of slip planes from the underlying substrate. No cracking was observed with mono-layer coatings whatever the applied strain. In contrast, after considerable straining of 20%, the thickest coatings exhibit some cracks along the slip lines on the substrate surface.

A scanning electron micrograph of the cracked coatings submitted to the scotch tape test is given in Fig. 6. It should be noted that cracking does not lead to a delamination within the coating or at the coating–substrate interface.

Keeping in mind that during cooling the coatings are submitted to a compressive stress due to the

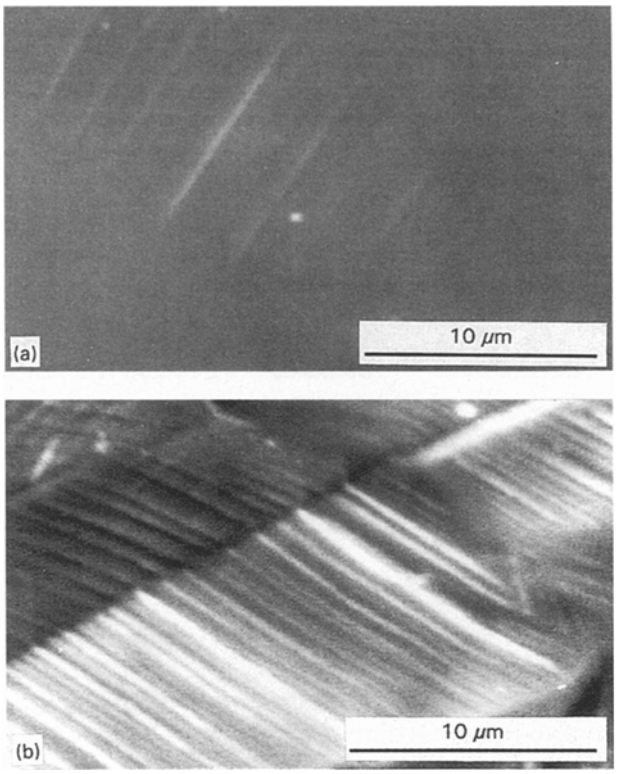

Figure 4 Scanning electron micrographs of zirconia mono-layer coatings after (a) 5% and (b) 20% elongation.

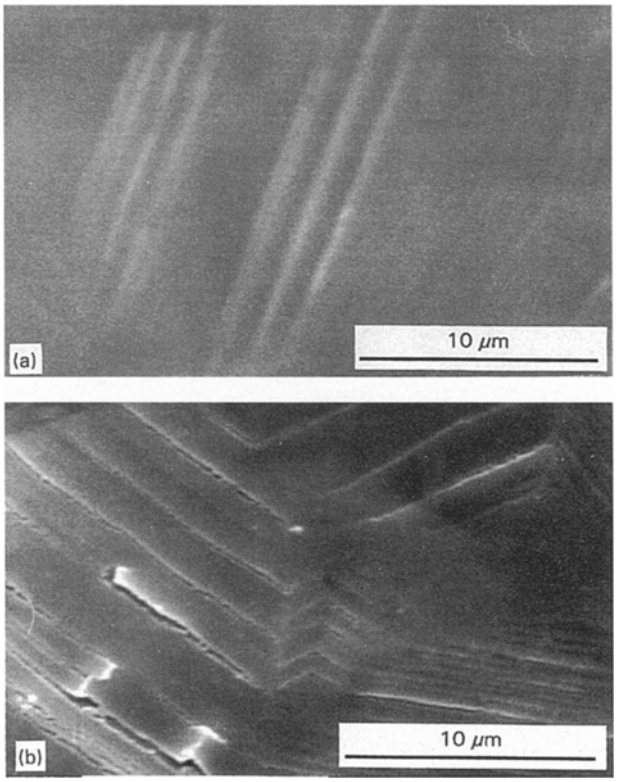

Figure 5 Scanning electron micrographs of zirconia four-layer coatings after (a) 5% and (b) 20% elongation.

thermal expansion mismatch [13] between zirconia ($\alpha = 10 \times 10^{-6\circ} C^{-1}$) and 304 stainless steel ($\alpha = 18 \times 10^{-6\circ} C^{-1}$) and taking into consideration the emergence of slip planes from the substrate under coatings during straining, the above results reveal that

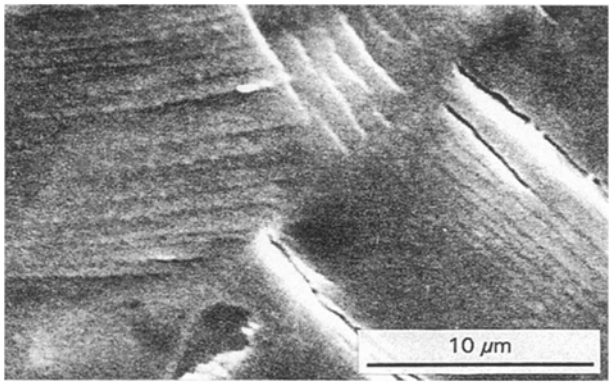

Figure 6 Scanning electron micrograph of zirconia four-layer coatings after 20% elongation and the subsequent scotch tape test.

the zirconia coatings exhibit both an unexpected elastic behaviour and a good adherence to the metallic substrate. These attractive properties can, respectively, be explained by the nanocrystalline structure [22] of the zirconia coatings and by the reaction of the Zr–OH or $Zr–OC_3H_7$ groups of the coating precursors with the –OH groups expected to be present on the oxidized metal surface.

3.3. Protective role

The electrodes under study were stainless steel plates successively coated with one, two, and four zirconia layers. The coating thickness as a function of the number of layers is given in Table II.

For the various electrodes, the values of the rest potential, E_a, and of the pitting potential, E_p, obtained before and after ageing in de-aerated NaCl solution are reported in Tables III–V. It can be observed that the rest potential of electrodes does not significantly vary with immersion time. The E_a values are lower than that measured for the uncoated stainless steel (− 114 mV/SCE) and close to that determined (− 190 mV/SCE) when it was heated in the same conditions as the coatings.

For a two-layer coating, it should be noted that the pitting potential of electrodes before ageing in chloride solution is much higher than that measured (300 mV/SCE) in the case of stainless steel neither coated, nor thermally treated. On the other hand, additional coating layers have little pronounced effect on the increase of the pitting potential.

The ageing treatment leads to a decrease of the pitting potential of the electrodes. The E_p values are shifted towards that obtained for the uncoated stainless steel but never reach that which was measured (− 70 mV/SCE) when it was treated thermally.

The behaviour of the electrodes during immersion in chloride solution with respect to pitting corrosion resistance reveals the presence of porosity within the coatings, which allows chloride ions to diffuse up to the zirconia–steel interface.

Fig. 7a shows two typical impedance diagrams, depressed semicircle (curve 2) and trend (curve 1) of a large capacitive loop, obtained, respectively, with stainless steel plates coated with one and four zirconia layers, before immersion in NaCl solution. These diagrams are formally represented by the electrical network sketched in Fig. 7b.

TABLE II Coating thickness as a function of number of zirconia layers

Layer number	Coating thickness (nm)
1	34
2	64
4	150

TABLE III Influence of immersion time on rest potential

Layer number	Initial rest potential (mV/SCE)	Immersion time (h)	Final rest potential (mV/SCE)
1	− 240	70	− 260
	− 200	130	− 260
2	− 180	60	− 140
	− 120	85	− 40
4	− 160	100	− 150
	− 190	100	− 150

TABLE IV Influence of layer number on pitting potential

Layer number	Pitting potential (mV/SCE)
1	210
2	700
4	800

TABLE V Influence of immersion time on pitting potential

Layer number	Immersion time (h)	Pitting potential (mV/SCE)
2	70	230
	100	220
	760	250
4	70	300
	80	340
	100	300
	170	400

The frequency distribution of the experimental points obeys the following equation

$$Z = R/1 + (j\omega RC)^{(1-\alpha)} \quad (1)$$

where R and C are, respectively, the resistance and the capacitance of the coating; the exponent α accounts for the deviation from the Debye dispersion.

The fitted parameters C, R and α deduced from the simulation, and hence the resistivity, ρ, and the dielectric constant, ε_r, are given in Table VI. The latter two parameters are, respectively, calculated from R and C values

$$\rho = RS/e \quad (2a)$$

$$\varepsilon_r = Ce/S\varepsilon_0 \quad (2b)$$

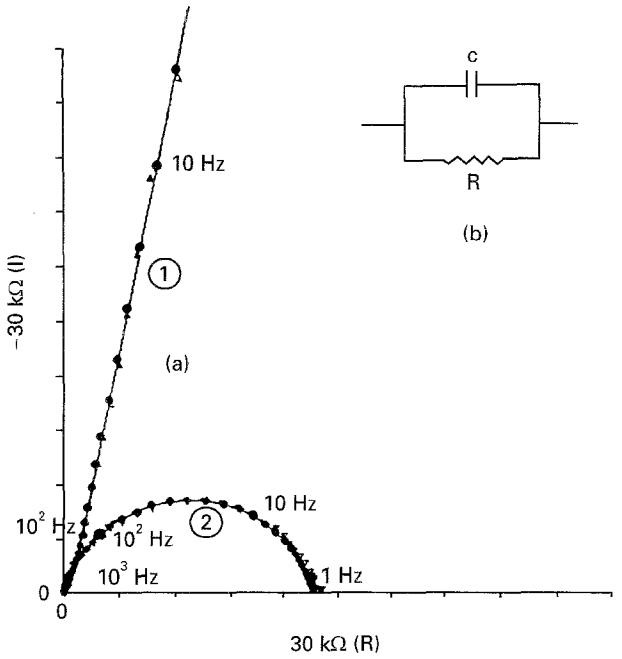

Figure 7 (a) Complex impedance diagrams obtained with stainless steel coated with zirconia layers: (1) Four zirconia layers, (2) one zirconia layer, (–●–) Fitting curves. (b) Electrical network.

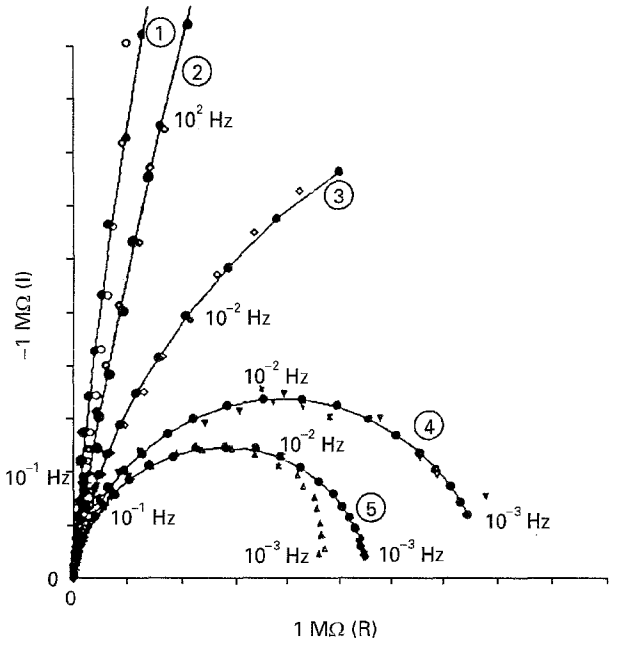

Figure 8 Complex impedance diagrams relative to stainless steel coated with four zirconia layers, immersed in neutral NaCl solutions: (1, 4, 5). immersion in aerated 0.5 M NaCl solution for 2 h, 10 days and 30 days successively; (3) immersion in aerated 0.02 M NaCl solution for 10 days; (2) immersion in de-aerated 0.5 M NaCl solution for 60 days; (–●–) fitting curves.

TABLE VI Fitting parameter variations with coating thickness

Layer number	$R(\Omega\,cm^2)$	$C(F\,cm^2)$	α	$\rho(\Omega\,cm)$	ε_r
1	1.37×10^4	1.2×10^{-6}	0.18	4×10^9	46
4	7×10^7	1.65×10^{-6}	0.12	4.7×10^{12}	280

with e, the coating thickness and S, the apparent area of electrode; S is equal to 1 cm^2.

The Nyquist diagrams recorded 2 h after the electrodes were immersed in NaCl solution still indicate only the HF trend of a large capacitive loop. For the samples coated with four zirconia layers, the evolution of this loop was studied as a function of experimental conditions (Fig. 8 and Table VII).

After ageing in aerated solution, a depressed semicircle is observed in the complex impedance diagram with a slight increase of the capacitance and a strong decrease of the resistance. It should be noted that this last evolution is quicker in aerated concentrated solutions. The rest potential decreases in aerated NaCl solution to the value obtained with thermally treated stainless steel.

In de-aerated 0.5 M NaCl solution, the complex impedance diagram recorded after subsequent exposure (60 days) presents no significant evolution of R and C parameters, the rest potential is stationary, and no delamination is observed.

The decrease of resistance values through ageing in a chloride-aerated medium could be ascribed to galvanic coupling inducing a delamination of the coating.

This damage is illustrated by scanning electron micrographs of electrodes previously immersed in aerated chloride medium for 1 and 2 months (Fig. 9): cracking and spalling of the zirconia coating are successively observed when the immersion time increases.

4. Conclusion

Nanocrystalline zirconia coatings on stainless steel were obtained from zirconium tetrabutoxide by firing

TABLE VII Fitting parameter variations with electrolytic medium and immersion time

Rest potential (mV/SCE)	R ($\Omega\,cm^2$)	C ($F\,cm^2$)	α	NaCl solution	Immersion time (day)
– 163	1.9×10^7	1.4×10^{-5}	0.05	0.5 M aerated	1
– 170	1.9×10^7	4.95×10^{-5}	0.09	0.5 M de-aerated	60
– 190	2.2×10^6	3.2×10^{-5}	0.1	0.02 M aerated	10
– 205	7.8×10^5	2.9×10^{-5}	0.09	0.5 M aerated	10
– 230	5.6×10^5	2.8×10^{-5}	0.08	0.5 M aerated	30

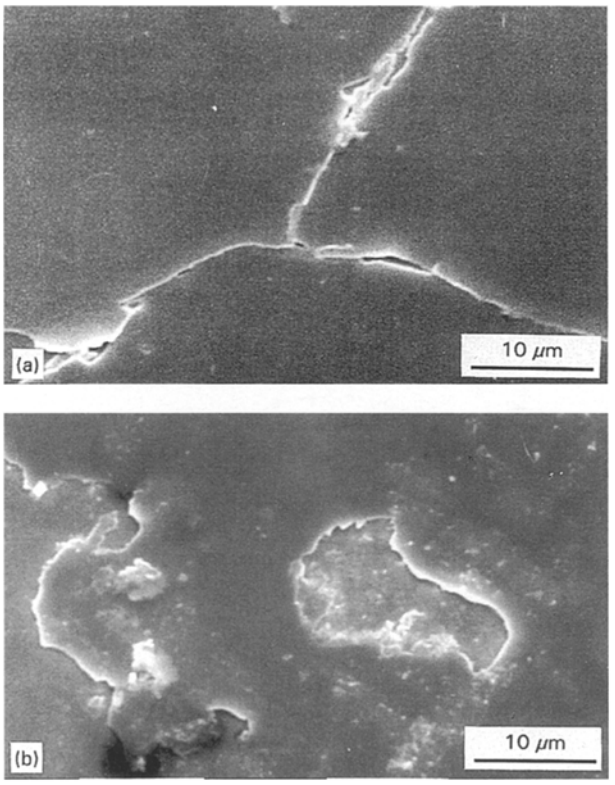

Figure 9 Scanning electron micrograph of electrodes after (a) 1 and (b) 2 months of immersion in chloride solution.

for 5 min at 500 °C. These coatings exhibit both an unexpected elastic behaviour and a good adherence to the metallic substrate. The corrosion behaviour of electrodes reveals the presence of porosity within coatings allowing oxygen to diffuse up to the zirconia–steel interface [19]. A porosity decrease should inhibit the delamination process.

References

1. H. DISLICH and E. HUSSMANN, *Thin Solid Films* **77** (1981) 129.
2. S. SAKKA, *J. Non-Cryst. Solids* **73** (1985) 651.
3. F. ORGAZ and H. RAWSON, *ibid.* **82** (1986) 378.
4. K. YAMADA, T. Y. CHOW, T. HORIHATA and M. NAGATA, *ibid.* **100** (1988) 316.
5. B. D. FABES and D. R. UHLMANN, *J. Am. Ceram. Soc.* **73** (1990) 978.
6. A. MATSUDA, Y. MATSUNO, S. KATAYAMA, T. TSUNO, N. TOHGE and T. MINAMI, *J. Ceram. Soc. Jpn* **99** (1991) 545.
7. R. L. NELSON, J. D. F. RAMSAY, J. L. WOODHEAD, J. A. CAIRNS and J. A. A. CROSSLEY, *Thin Solid Films* **81** (1981) 329.
8. M. J. BENNETT, *J. Vac. Sci. Technol.* **2** (1984) 800.
9. N. TOHGE, A. MATSUDA and T. MINAMI, *Chem. Express* **2** (3) (1987) 141.
10. L. YANG and J. CHENG, *J. Non-Cryst. Solids* **112** (1989) 442.
11. K. IZUMI, M. MURAKAMI, T. DEGUCHI, A. MORITA, N. TOHGE and T. MINAMI, *J. Am. Ceram. Soc.* **72** (1989) 1465.
12. O. DESANCTIS, L. GOMEZ, N. PELLEGRI, C. PARODI, A. MARAJOFSKI and A. DURAN, *J. Non-Cryst. Solids* **121** (1990) 338.
13. M. SHANE and M. L. MECARTNEY, *J. Mater. Sci.* **25** (1990) 1537.
14. L. J. De VORE and N. R. OSBORN, in "Better Ceramics Through Chemistry", Materials Research Society Symposium Proceedings, Vol. 180 (1990) p. 473.
15. R. Di MAGGIO, P. SCARDI and A. TOMASI, *ibid.* Vol. 180 (1990) p. 481.
16. A. R. Di GIAMPAOLO CONDE, M. PUERTA, H. RUIZ, and J. LIRA OLIVARES, *J. Non-Cryst. Solids* **147/148** (1992) 467.
17. M. GUGLIELMI, D. FESTA, P. C. INNOCENTI, P. COLOMBO and M. GOBBIN, *ibid.* **147/148** (1992) 474.
18. M. ATIK and M. A. AEGERTER, *ibid.* **147/148** (1992) 813.
19. J. F. QUINSON, C. CHINO, A. M. de BECDELIEVRE and C. GUIZARD, in "Better Ceramics Through Chemistry", Materials Research Society Symposium Proceedings, Vol. 346 (1994) p. 703.
20. B. E. YOLDAS, *J. Am. Ceram. Soc.* **65** (1982) 387.
21. Y. ARNAUD, M. BRUNEL, A. M. de BECDELIEVRE, M. ROMAND, P. THEVENARD and M. ROBELET, *Appl. Surf. Lett.* **26** (1986) 12.
22. H. E. SCHAEFER, R. WÛRSCHUM, R. BIRRINGER and H. GLEITER, *J. Less-Common Metals* **140** (1988) 161.
23. H. GLEITER, *Adv. Mater.* **4** (1992) 474.
24. R. W. SIEGEL, in "Materials Interfaces", edited by D. Wolf and S. Yip (Chapman and Hall, London, 1992) p. 431.

Received 4 April
and accepted 20 November 1995